

A Modified Magnitude-Selective Affine Function-Based Behavioral Digital Predistortion for Power Amplifiers in MIMO Systems

Haopu Shen, Cuiping Yu*, Ke Tang, and Yuanan Liu

Abstract—In this paper, a modified magnitude-selective affine function-based behavioral model is proposed for the linearization of power amplifiers in multiple-input multiple-output (MIMO) systems. In this model, high-order polynomials in the crossover memory polynomial (COMPM) are replaced by magnitude-selective affine functions to compensate for the crosstalk and nonlinear distortion, leading to a highly efficient hardware implementation. The performance of the model is validated using two 3-carrier long-term evolution (LTE) signals of 20 MHz bandwidth. Experimental results show that the proposed model can achieve nearly the same adjacent channel power ratio (ACPR) and normalized mean square error (NMSE) as COMPM with about 70% reduction of hardware complexity.

1. INTRODUCTION

To meet the needs of high rate and large-capacity communication needs, multiple-input multiple-output (MIMO) technique has become an essential part of the current fifth-generation (5G) wireless communication due to its inherent advantages [1]. However, in MIMO system, the multiple RF channels may be placed closely, or even be integrated on the same chip, which will introduce crosstalk between channels. The crosstalk leads to the generation of new nonlinear distortion when it passes through power amplifiers (PAs), which degrades the quality of the output signal and also brings great challenges to the linearization of the PAs [2].

Digital predistortion (DPD) has been widely adopted for the compensation of transmitter nonlinearities in wireless communication system. In the presence of crosstalk, conventional DPD algorithms cannot compensate the nonlinearities generated by the PAs. Thus, many different DPD models suitable for MIMO systems have been proposed in recent years. In [4], a crossover memory polynomial (COMPM) is firstly proposed to compensate for crosstalk and nonlinearity in MIMO systems. In this model, the output of the PA is approximated as the sum of two nonlinear functions. In [5], Saffar et al. proposed a 2×2 Parallel Hammerstein (2×2 PH) model, which can achieve better linearization performance than COMPM. However, the existence of triple summation symbols leads to a huge number of coefficients, which will consume a lot of computing resources. In [6] and [7], the models reduce the quantity of the coefficients to reduce complexity by modifying the basis functions, which can achieve approximate linearization performance at a lower number of coefficients than 2×2 PH. In [8], a dual-input crosstalk mismatch model (DI-CTMM) for multi-antenna transmitters has been proposed. This model compensates for the combined effects of PAs, antenna crosstalk, and impedance with a linear crosstalk and mismatch model block shared by all transmitting paths and a dual-input DPD block in every transmitting path. However, when it comes to multiple channels, the coefficients of these models will increase rapidly, which will consume huge hardware resources. As a consequence, a low-complexity DPD model is of great importance for MIMO systems. The proposed model is to

Received 2 June 2022, Accepted 9 August 2022, Scheduled 13 September 2022

* Corresponding author: Cuiping Yu (yucuiping@bupt.edu.cn).

The authors are with the Beijing Key Laboratory of Work Safety Intelligent Monitoring, Beijing University of Posts and Telecommunications, Beijing 100876, China.

further reduce the hardware complexity on the basis of the existing low-complexity DPD model suitable for MIMO systems.

The magnitude-selective affine (MSA) function-based DPD was proposed for 5G small-cell transmitters [9, 10]. In this model, the cross-terms are redesigned by magnitude-selective affine functions to construct nonlinear behavior of the model. Partial complex multiplication is replaced by complex addition, which can achieve the significant reduction of hardware resources. In this paper, MSA function-based DPD is applied to MIMO systems, and MSA functions are used to replace the high-order polynomials in COMPM. This paper is organized as follows. In Section 2, after a brief review of COMPM, the proposed model is introduced in detail. The performance of the proposed model is verified through experiments in Section 3. Finally, Section 4 is the conclusion.

2. THE PROPOSED MODEL

In MIMO systems, according to the location where the crosstalk occurs, the crosstalk can be divided into linear crosstalk and nonlinear crosstalk. Fig. 1 shows the MIMO transmitters with linear crosstalk and nonlinear crosstalk, where coupling factors α and β denote the effects of nonlinear crosstalk, and γ and δ denote the effects of linear crosstalk. It can be seen that the input signals and output signals can be coupled with each other, which means that the output of the power amplifier will be affected not only by one input signal, but also by another.

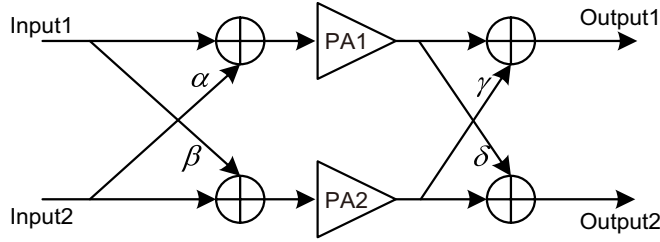


Figure 1. Block diagram of a 2×2 MIMO transmitter with linear and nonlinear crosstalk.

In [3], COMPM is proposed to compensate for crosstalk and nonlinearity in MIMO systems, and the output of a transmitter path in 2×2 COMPM is mathematically expressed as

$$y_r(n) = \sum_{q=0}^{Q-1} \sum_{p=0}^{P-1} \alpha_{p,q}^{(r)} x_r(n-q) |x_r(n-q)|^p + \sum_{q=0}^{Q-1} \sum_{p=0}^{P-1} b_{p,q}^{(r)} x_s(n-q) |x_s(n-q)|^p \quad (1)$$

where $y_r(n)$ is the output of the first power amplifier, herein, $r, s \in \{1, 2\}$ and $r \neq s$; $\alpha_{p,q}^{(r)}$ and $b_{p,q}^{(r)}$ are the coefficients of the model; $x_1(n)$ and $x_2(n)$ are the inputs; Q is the memory depth; P is the nonlinear order.

In order to further reduce the complexity of hardware implementation, it should be possible to replace the multiplication with other more efficient operations. Then MSA function-based behavioral model is used to the model construction in MIMO systems. The proposed model is shown in the following expression:

$$y_1(n) = \sum_{m=0}^{M-1} u_{1m}(n-m) e^{j\theta_1(n-m)} + \sum_{m=0}^{M-1} u_{2m}(n-m) e^{j\theta_2(n-m)} \quad (2)$$

where M is the memory depth, and $\theta_1(n)$ and $\theta_2(n)$ are the phases of $x_1(n)$ and $x_2(n)$, respectively.

u_{1m} and u_{2m} can be written as follows:

$$u_{1m}(n-m) = \begin{cases} f_{1m}^{(1)}(|x_1(n-m)|), & 0 \leq |x_1(n)| < \beta_1 \text{ \& } 0 \leq |x_2(n)| < \beta_1 \\ f_{2m}^{(1)}(|x_1(n-m)|), & 0 \leq |x_1(n)| < \beta_1 \text{ \& } \beta_1 \leq |x_2(n)| < \beta_2 \\ \vdots \\ f_{Km}^{(1)}(|x_1(n-m)|), & 0 \leq |x_1(n)| < \beta_1 \text{ \& } \beta_{K-1} \leq |x_2(n)| < \beta_K \\ \vdots \\ f_{(K^2-1)m}^{(1)}(|x_1(n-m)|), & \beta_{K-1} \leq |x_1(n)| < \beta_K \text{ \& } \beta_{K-2} \leq |x_2(n)| < \beta_{K-1} \\ f_{K^2m}^{(1)}(|x_1(n-m)|), & \beta_{K-1} \leq |x_1(n)| < \beta_K \text{ \& } \beta_{K-1} \leq |x_2(n)| < \beta_K \end{cases} \quad (3)$$

$$u_{2m}(n-m) = \begin{cases} f_{1m}^{(2)}(|x_2(n-m)|), & 0 \leq |x_1(n)| < \beta_1 \text{ \& } 0 \leq |x_2(n)| < \beta_1 \\ f_{2m}^{(2)}(|x_2(n-m)|), & 0 \leq |x_1(n)| < \beta_1 \text{ \& } \beta_1 \leq |x_2(n)| < \beta_2 \\ \vdots \\ f_{Km}^{(2)}(|x_2(n-m)|), & 0 \leq |x_1(n)| < \beta_1 \text{ \& } \beta_{K-1} \leq |x_2(n)| < \beta_K \\ \vdots \\ f_{(K^2-1)m}^{(2)}(|x_2(n-m)|), & \beta_{K-1} \leq |x_1(n)| < \beta_K \text{ \& } \beta_{K-2} \leq |x_2(n)| < \beta_{K-1} \\ f_{K^2m}^{(2)}(|x_2(n-m)|), & \beta_{K-1} \leq |x_1(n)| < \beta_K \text{ \& } \beta_{K-1} \leq |x_2(n)| < \beta_K \end{cases} \quad (4)$$

where β_k ($k = 1, 2, 3, \dots, K$; $\beta_k = k/K$) is the threshold value that divides the two input envelope magnitude ranges into K^2 partitions. $f_{im}^{(1)}$ and $f_{im}^{(2)}$ can be written as:

$$f_{jm}^{(i)}(|x_1(n-m)|) = A_{jm}^{(i)} |x_1(n-m)| + B_{jm}^{(i)} \quad (5)$$

where $A_{jm}^{(i)}$ and $B_{jm}^{(i)}$ are the model coefficients ($i = 1, 2$; $j = 1, 2, 3, \dots, K^2 - 1, K^2$).

The implementations of the proposed model for the two transmitter paths are nearly the same. Take the first path as an example. Fig. 2 depicts the construction of the proposed model. Fig. 3 shows

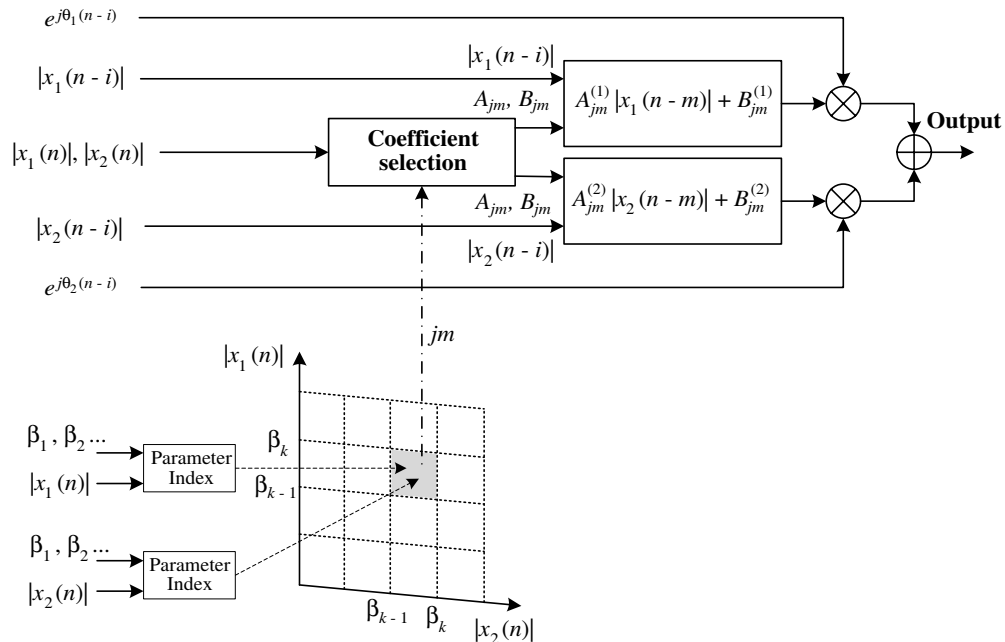


Figure 2. Construction of the proposed model.

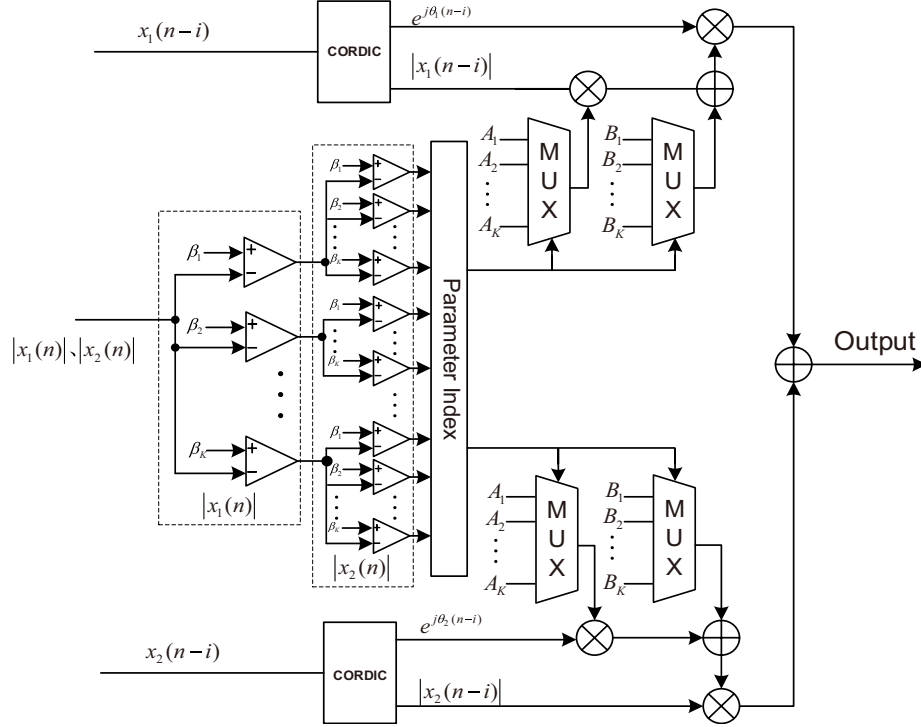


Figure 3. Hardware implementation of the proposed model.

the hardware implementation example of the first transmitter path. The two input complex signals are first decomposed into magnitude and phase respectively using the coordinate rotation digital computer (CORDIC) algorithm. Then, the magnitudes of two input signals are compared with the threshold values to choose the model coefficients. After the process of coefficient selection, the coefficients are multiplied with or added to their corresponding input magnitudes, and the phase of each signal is then restored by multiplying with $e^{j\theta_1(n-i)}$ and $e^{j\theta_2(n-i)}$, respectively. The output can be obtained by adding them together.

In the proposed model, the high-order polynomials in COMPM are replaced by MSA functions, which can save lots of hardware resources.

3. COMPLEXITY REDUCTION IN MODEL EXTRACTION

The proposed model maintains the linear characteristics of the parameters, so the model coefficients can be extracted by the least squares (LS) method. The proposed model in matrix format is written as

$$\mathbf{Y}_{N \times 1}^{(i)} = \mathbf{X}_{N \times R}^{(i)} \mathbf{W}_{R \times 1}^{(i)} \quad i = 1, 2 \quad (6)$$

where $i = 1, 2$ is used to represent the different transmitter paths. \mathbf{X} is the input matrix of the PA; \mathbf{Y} is the corresponding output vector; and \mathbf{W} includes all the coefficients. The subscript R is the total number of the coefficients, and N is the number of samples.

For simplicity, the memory depth M is set to 1, and the number of thresholds is set to 2 as an example. The model can be expressed as

$$\begin{aligned} y(n) &= \left(A_{j_0}^{(1)} |x_1(n)| + B_{j_0}^{(1)} \right) e^{j\theta_1(n)} + \left(A_{j_0}^{(2)} |x_2(n)| + B_{j_0}^{(2)} \right) e^{j\theta_2(n)} \\ &= A_{j_0}^{(1)} x_1(n) + B_{j_0}^{(1)} e^{j\theta_1(n)} + A_{j_0}^{(2)} x_2(n) + B_{j_0}^{(2)} e^{j\theta_2(n)} \end{aligned} \quad (7)$$

where $A_{j_0}^{(1)}$, $B_{j_0}^{(1)}$, $A_{j_0}^{(2)}$, and $B_{j_0}^{(2)}$ are the model coefficients. From (7), it is clear that there are only four active coefficients used, but because there are four partitions, the total number of coefficients is 16.

Two sets of input sample sequences are given for example, $x_1 = [x_1(0), x_1(1), \dots, x_1(7)]^T$ and $x_2 = [x_2(0), x_2(1), \dots, x_2(7)]^T$, and the corresponding output samples sequences of transmitter paths are denoted as y_1 and y_2 . Fig. 4 shows the segmentation results of the two input samples. The matrix $X^{(1)}$ can be written as

$$X^{(1)} = \begin{bmatrix} x_1(0) & e^{j\theta_{10}} & x_2(0) & e^{j\theta_{20}} & 0 & 0 & 0 & 0 & 0 & 0 & 0 & 0 & 0 & 0 & 0 & 0 \\ x_1(1) & e^{j\theta_{11}} & x_2(1) & e^{j\theta_{21}} & 0 & 0 & 0 & 0 & 0 & 0 & 0 & 0 & 0 & 0 & 0 & 0 \\ 0 & 0 & 0 & 0 & 0 & 0 & 0 & 0 & x_1(2) & e^{j\theta_{12}} & x_2(2) & e^{j\theta_{22}} & 0 & 0 & 0 & 0 \\ 0 & 0 & 0 & 0 & 0 & 0 & 0 & 0 & 0 & 0 & 0 & 0 & x_1(3) & e^{j\theta_{13}} & x_2(3) & e^{j\theta_{23}} \\ 0 & 0 & 0 & 0 & x_1(4) & e^{j\theta_{14}} & x_2(4) & e^{j\theta_{24}} & 0 & 0 & 0 & 0 & 0 & 0 & 0 & 0 \\ 0 & 0 & 0 & 0 & 0 & 0 & 0 & 0 & 0 & 0 & 0 & 0 & x_1(5) & e^{j\theta_{15}} & x_2(5) & e^{j\theta_{25}} \\ 0 & 0 & 0 & 0 & 0 & 0 & 0 & 0 & x_1(6) & e^{j\theta_{16}} & x_2(6) & e^{j\theta_{26}} & 0 & 0 & 0 & 0 \\ 0 & 0 & 0 & 0 & x_1(7) & e^{j\theta_{17}} & x_2(7) & e^{j\theta_{27}} & 0 & 0 & 0 & 0 & 0 & 0 & 0 & 0 \end{bmatrix}$$

where the values of the inactive elements are set as 0. Once the matrix $X^{(1)}$ is obtained, the LS algorithm can be used directly to extract the coefficients. Since the size of $X^{(1)}$ is too large, the matrix operations will be costly.

In order to simplify the process of model extraction, the method in [9] can be applied to divide the large matrix into several small matrices. The model coefficients of the same small area are unique, and they are completely determined by the input samples that fall in this area and will not be influenced by other samples.

According to the segmentation results of the two input samples in Fig. 4, large matrix operation can be broken into four smaller operations as follows:

$$\begin{aligned} \text{area 1 : } \begin{bmatrix} y_1(0) \\ y_1(1) \end{bmatrix} &= \begin{bmatrix} x_1(0) & e^{j\theta_{10}} & x_2(0) & e^{j\theta_{20}} \\ x_1(1) & e^{j\theta_{11}} & x_2(1) & e^{j\theta_{21}} \end{bmatrix} \begin{bmatrix} A_{10}^{(1)} \\ B_{10}^{(1)} \\ A_{10}^{(2)} \\ B_{10}^{(2)} \end{bmatrix} \\ \text{area 2 : } \begin{bmatrix} y_1(4) \\ y_1(7) \end{bmatrix} &= \begin{bmatrix} x_1(4) & e^{j\theta_{14}} & x_2(4) & e^{j\theta_{24}} \\ x_1(7) & e^{j\theta_{17}} & x_2(7) & e^{j\theta_{27}} \end{bmatrix} \begin{bmatrix} A_{20}^{(1)} \\ B_{20}^{(1)} \\ A_{20}^{(2)} \\ B_{20}^{(2)} \end{bmatrix} \\ \text{area 3 : } \begin{bmatrix} y_1(2) \\ y_1(6) \end{bmatrix} &= \begin{bmatrix} x_1(2) & e^{j\theta_{12}} & x_2(2) & e^{j\theta_{22}} \\ x_1(6) & e^{j\theta_{16}} & x_2(6) & e^{j\theta_{26}} \end{bmatrix} \begin{bmatrix} A_{30}^{(1)} \\ B_{30}^{(1)} \\ A_{30}^{(2)} \\ B_{30}^{(2)} \end{bmatrix} \\ \text{area 4 : } \begin{bmatrix} y_1(3) \\ y_1(5) \end{bmatrix} &= \begin{bmatrix} x_1(3) & e^{j\theta_{13}} & x_2(3) & e^{j\theta_{23}} \\ x_1(5) & e^{j\theta_{15}} & x_2(5) & e^{j\theta_{25}} \end{bmatrix} \begin{bmatrix} A_{40}^{(1)} \\ B_{40}^{(1)} \\ A_{40}^{(2)} \\ B_{40}^{(2)} \end{bmatrix} \end{aligned}$$

To generalize this property, the matrix representation in (6) can be decomposed into a submatrix representation

$$\begin{cases} Y_1^{(i)} = X_1^{(i)} W_1^{(i)} \\ Y_2^{(i)} = X_2^{(i)} W_2^{(i)} \\ \dots \\ Y_{K^2}^{(i)} = X_{K^2}^{(i)} W_{K^2}^{(i)} \end{cases} \quad (i = 1, 2) \quad (8)$$

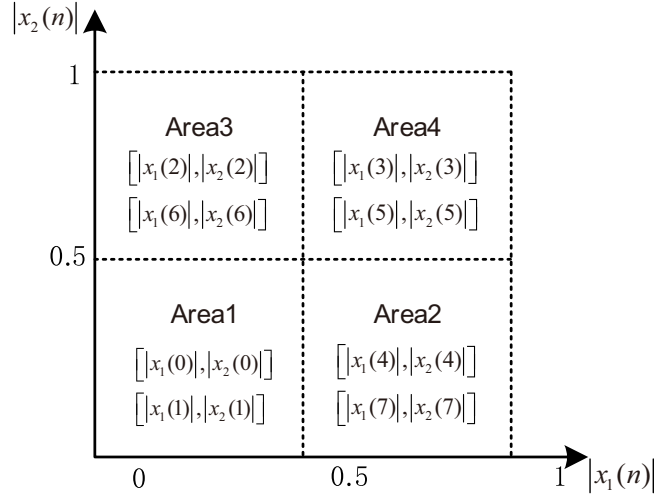


Figure 4. Segmentation results of the sample sequences.

where $Y_k^{(i)}$, $X_k^{(i)}$, and $W_k^{(i)}$ represent the corresponding output vector, the matrix of input signals, and coefficients vector in the k th area, respectively. The coefficients vector of different areas can be obtained by LS algorithm respectively.

$$\begin{cases} W_1^{(i)} = \left(X_1^{(i)H} X_1^{(i)} \right)^{-1} X_1^{(i)H} Y_1^{(i)} \\ W_2^{(i)} = \left(X_2^{(i)H} X_2^{(i)} \right)^{-1} X_2^{(i)H} Y_2^{(i)} \\ \dots \\ W_{K^2}^{(i)} = \left(X_{K^2}^{(i)H} X_{K^2}^{(i)} \right)^{-1} X_{K^2}^{(i)H} Y_{K^2}^{(i)} \end{cases} \quad (9)$$

The complexity of the least squares calculation in (6) is proportional to R^2N . When it comes to (9), the complexity can be expressed by

$$\sum_{k=1}^{K^2} \left(\frac{R}{K^2} \right)^2 N_k = \frac{R^2N}{K^4} \quad (10)$$

where N_k is the number of samples in area k , which satisfies $\sum_{k=1}^{K^2} N_k = N$.

In the proposed model, the number of coefficients will increase slightly, but the computational complexity will be reduced significantly because the matrix dimension used to extract coefficients for the LS method becomes smaller.

4. MEASUREMENT RESULTS

In this section, the performance of the proposed model is verified and compared with the COMPM. The measurement setup of the 2×2 MIMO system is shown in Fig. 5. The setup consists of two vector signal generators (AgilentMXG N5182A and Agilent ESG E4438C), a baseband generator and channel emulator (Agilent PXB N5106A), two power amplifiers, two couplers, a vector & spectrum signal analyzer (R&S FSW43), and a PC. Two 3-carrier LTE signals of 60 MHz bandwidth signals with 7.1 dB peak-to-average power ratio (PAPR) are considered as the input signals. The output signals were sampled at a sample rate of 200 MHz and were sent at a carrier frequency of 2.3 GHz using two signal generators connected to a computer.

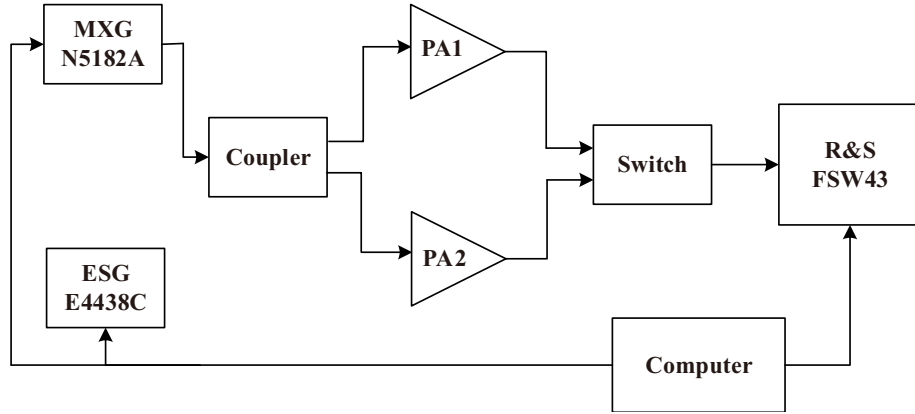


Figure 5. Block diagram of experimental setup.

To introduce crosstalk, these two RF signals were passed through couplers of -20 dB coupling factor. After that, the PAs were driven by these RF signals. The output RF signals from couplers were passed through attenuators and then captured by digital signal analyzer.

To verify the performance of the proposed model, COMPM was measured for comparison. K of the proposed model used in the experiment is set to 4, and M is set to 3. In the proposed model, K is used for segmentation. The parameters of Single-Input Single-Output (SISO) model and COMPM were set to $P = 5$ and $Q = 3$. Under the parameter conditions given, all of the models can achieve the best performance. The linearization performance of different DPD methods is evaluated in terms of NMSE and ACPR. They are summarized in Table 1 and Table 2. Fig. 6 shows the power spectral density of the two PAs' output signals. In this paper, the hardware complexity of the proposed has been evaluated by Floating Point Operations (FLOPs). It has been calculated and listed in Table 1. From the tables, it can be seen that the proposed model can achieve nearly the same ACPR and NMSE as the COMPM with about 70% reduction of FLOPs. Compared with SISO model, the ACPR of the proposed model is improved by about 5 dB/3 dB, and the NMSE is improved by 14 dB/10 dB with the FLOPs reduced from 272 to 168. The experimental results have proved the effectiveness of the proposed model.

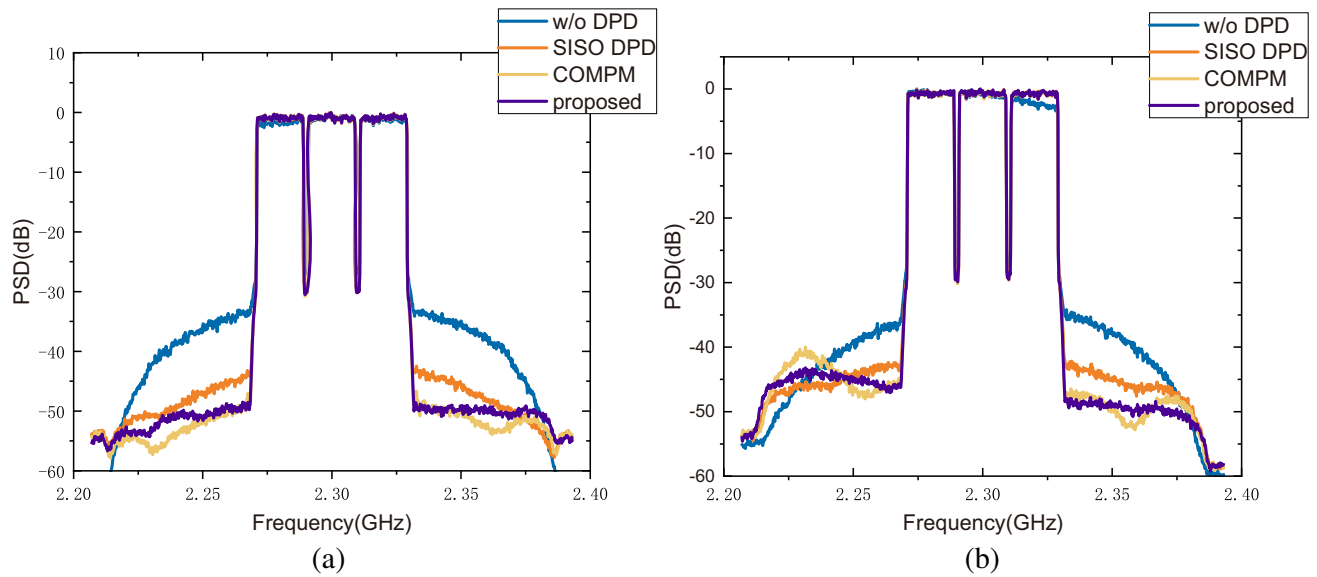


Figure 6. Power spectral density of various DPD methods' output for different PAs. (a) PA1, (b) PA2.

Table 1. DPD results for different methods.

Models	ACPR(PA1) (dBc)		ACPR(PA2) (dBc)		FLOPs
w/o DPD	-33.44	-33.23	-36.69	-35.33	/
SISO DPD	-44.21	-43.30	-42.64	-42.83	272
COMP	-48.91	-48.36	-45.60	-46.88	568
proposed	-48.48	-48.42	-45.05	-47.81	168

Table 2. NMSE for different methods.

Models	NMSE(PA1) (dB)	NMSE(PA2) (dB)
w/o DPD	-18.96	-16.62
SISO DPD	-20.16	-18.50
COMP	-34.23	-28.43
proposed	-34.13	-28.44

5. CONCLUSION

In this paper, a modified magnitude-selective affine function-based model is proposed for the linearization of power amplifiers in MIMO systems, which can compensate for the crosstalk and nonlinear distortion effectively. This model can also reduce the hardware complexity significantly. The performance of the proposed model has been verified by experimental results. The experimental results show that the proposed model can achieve the ACPR and NMSE performance close to the COMP with the 70% reduction of FLOPs. It is predictable that low cost hardware implementation and great linearization performance make the proposed model a competitive candidate for MIMO DPD solutions in the future wireless systems.

ACKNOWLEDGMENT

This work was supported by the Fundamental Research Funds for the Central Universities of Beijing University of Posts and Telecommunications, and National Natural Science Foundation of China (No. 61922016 and No. 62090015).

REFERENCES

1. Larsson, E. G., O. Edfors, F. Tufvesson, and T. L. Marzetta, "Massive MIMO for next generation wireless systems," *IEEE Communications Magazine*, Vol. 52, No. 2, 186–195, Feb. 2014.
2. Palaskas, Y., et al., "A 5-GHz 108-Mb/s 2×2 MIMO transceiver RFIC with fully integrated 20.5-dBm power P1 dB amplifiers in 90-nm CMOS," *IEEE J. Solid-State Circuits*, Vol. 41, No. 12, 2746–2756, Dec. 2006.
3. Ding, L., et al., "A robust digital baseband predistorter constructed using memory polynomials," *IEEE Transactions on Communications*, Vol. 52, No. 1, 159–165, Jan. 2004.
4. Bassam, S. A., M. Helaoui, and F. M. Ghannouchi, "Crossover digital predistorter for the compensation of crosstalk and nonlinearity in MIMO transmitters," *IEEE Transactions on Microwave Theory and Techniques*, Vol. 57, No. 5, 1119–1128, May 2009.
5. Saffar, D., N. Boulejeff, F. M. Ghannouchi, A. Gharsallah, and M. Helaoui, "Behavioral modeling of MIMO nonlinear systems with multivariable polynomials," *IEEE Transactions on Microwave Theory and Techniques*, Vol. 59, No. 11, 2994–3003, Nov. 2011.

6. Abdelhafiz, A., L. Behjat, F. M. Ghannouchi, M. Helaoui, and O. Hammi, "A high-performance complexity reduced behavioral model and digital predistorter for MIMO systems with crosstalk," *IEEE Transactions on Communications*, Vol. 64, No. 5, 1996–2004, May 2016.
7. Jaraut, P., M. Rawat, and F. M. Ghannouchi, "Curtailed digital predistortion model for crosstalk in MIMO transmitters," *2018 IEEE/MTT-S International Microwave Symposium — IMS*, 2018.
8. Hausmair, K., P. N. Landin, U. Gustavsson, C. Fager, and T. Eriksson, "Digital predistortion for multi-antenna transmitters affected by antenna crosstalk," *IEEE Transactions on Microwave Theory and Techniques*, Vol. 66, No. 3, 1524–1535, Mar. 2018.
9. Li, Y., W. Cao, and A. Zhu, "Instantaneous sample indexed magnitude-selective affine function-based behavioral model for digital predistortion of RF power amplifiers," *IEEE Transactions on Microwave Theory and Techniques*, Vol. 66, No. 11, 5000–5010, Nov. 2018.
10. Chen, L., W. Chen, F. M. Ghannouchi, and Z. Feng, "2-D magnitude-selective affine function-based digital predistortion for concurrent dual-band terminal power amplifiers," *IEEE Transactions on Microwave Theory and Techniques*, Vol. 69, No. 9, 4209–4222, Sept. 2021.